How to cite: *Angew. Chem. Int. Ed.* **2020**, *59*, 13328–13334
International Edition: doi.org/10.1002/anie.202003512
German Edition: doi.org/10.1002/ange.202003512

Supramolecular Chemistry

Polypyridine-Based Helical Amide Foldamer Channels: Rapid Transport of Water and Protons with High Ion Rejection

*Jie Shen, Jingrong Fan, Ruijuan Ye, Ning Li, Yuguang Mu, and Huaqiang Zeng**

Abstract: *Synthetic strategies that enable rapid construction of covalent organic nanotubes with an angstrom-scale tubular pore remain scarcely reported. Reported here is a remarkably simple and mild one-pot polymerization protocol, employing $POCl_3$ as the polymerization agent. This protocol efficiently generates polypyridine amide foldamer-based covalent organic nanotubes with a 2.8 nm length at a yield of 50 %. Trapping single-file water chains in the 2.8 Å tubular cavity, rich in hydrogen-bond donors and acceptors, these tubular polypyridine ensembles rapidly and selectively transport water at a rate of 1.6×10^9 $H_2O \cdot S^{-1} \cdot channel^{-1}$ and protons at a speed as fast as gramicidin A, with a high rejection of ions.*

Introduction

Organic nanotubes (ONTs), possessing a sizable hollow tubular cavity at the angstrom/nanometer-scale, are a class of structurally fascinating and functionally exciting molecules.[1] Current efforts toward rapid construction of long covalent ONTs with an angstrom-scale precision cavity largely rely on the light-promoted crosslinking of macrocycles,[2a–c] helices,[2d,e] or porphyrin dendrimers.[2f] Given that the crosslinking process will unavoidably result in structural distortion, with incomplete and various extents of crosslinking, the produced covalent ONTs are actually a mixture with significant heterogeneities in pore size amongst and within any single ONT. This heterogeneity may be problematic when highly selective molecular transport is desired. Other endeavours employed electrostatic repulsions among adjacent electron-rich heteroatoms to drive the formation of foldamer-based long covalent ONTs.[3]

Pioneered by the groups of Hamilton,[4a] Gong,[4b] and Lehn,[4c] hydrogen-bonded aromatic amide foldamers[1b,f,l,5] are the most studied among aromatic foldamers driven by noncovalent forces.[6] Because these helically folded aromatic amide backbones are fully rigidified by intramolecular hydrogen bonds and further stabilized by extensive π–π stacking forces, they could remain helically folded even in the aqueous solution.[7] Further, they are favourably characterized by high predictability in folding structure and uniform cavity size from constituent helicity codons as well as amenability to exterior modifications. After 25 years of research, a broad variety of helicity codons with built-in hydrogen-bonding capacity have been invented to generate an extremely broad range of fully hydrogen-bonded amide foldamers, enclosing sizable cavities ranging from 2.8 to 30 Å in diameter[5f–i] or far beyond. Hence, the advent of these hydrogen-bonded aromatic amide foldamers offers promising aspects in creating stably folded covalent ONTs of uniform pore size that is additionally adjustable. Yet, these attractive features are offset by synthetically demanding and painstaking stepwise preparation of hydrogen-bonded long ONTs of three or more helical turns and a greater than or equal to 1 nm helical height.

As such, one-pot polymerization has been pursued as a logical alternative to achieve efficient synthesis of long covalent ONTs derived from hydrogen-bonded aromatic amide foldamers.[1d,e] Presumably arising from the backbone rigidity induced low reactivities of the amines and carboxylic acids, such one-pot polymerization endeavors have so far not been successful, generating only short fully hydrogen-bonded ONTs of average tubular lengths less than or equal to 1.1 nm.[1d,e] The rigidity-induced low reactivity can be evidenced by the fact that, upon partial relaxation of the hydrogen-bonded rigid backbone by eliminating 50 % intramolecular hydrogen bonds, the polymerized partially hydrogen-bonded ONTs have a helical length of up to 6.1 nm.[8] These partially relaxed ONTs, however, are accompanied by substantially decreased helical robustness. As such, except for significant contributions on long aromatic amide foldamers by the group of Huc,[1f] investigations on the majority of diverse hydrogen-bonded aromatic amide foldamers have predominantly focused on short oligomers of less than 1 nm in helical height,[1b,f,l,4,5] greatly limiting the functional potential of the aromatic amide foldamers in various fields.

Previously, we reported a series of hydrogen-bonded pyridine-based aromatic foldamers, containing up to five repeating units (e.g., **1** from Figure 1 a).[9] These oligopyridine foldamers require about 4.3 residues to form a helical turn,[9a] which, after excluding van der Waals radii of the interior-pointing amide H atoms, generates a cavity of about 2.8 Å across. Importantly, this small cavity, which is decorated by many hydrogen-bond donors and acceptors, matches well with the diameter of a water molecule. Accordingly, pyridine pentamers such as **1** take a helically folded structure (Figure 1 a).[9d–f] Upon introducing two "sticky ends" at helical

[*] Dr. J. Shen, Dr. N. Li, Dr. H. Zeng
The NanoBio Lab
31 Biopolis Way, The Nanos, Singapore 138669 (Singapore)
E-mail: hqzeng@nbl.a-star.edu.sg
R. Ye
Department of Chemical and Biomolecular Engineering, National University of Singapore
Singapore 117585 (Singapore)
Dr. J. Fan, Prof. Y. Mu
School of Biological Sciences, Nanyang Technological University
Singapore 637551 (Singapore)
Supporting information and the ORCID identification number(s) for the author(s) of this article can be found under: https://doi.org/10.1002/anie.202003512.

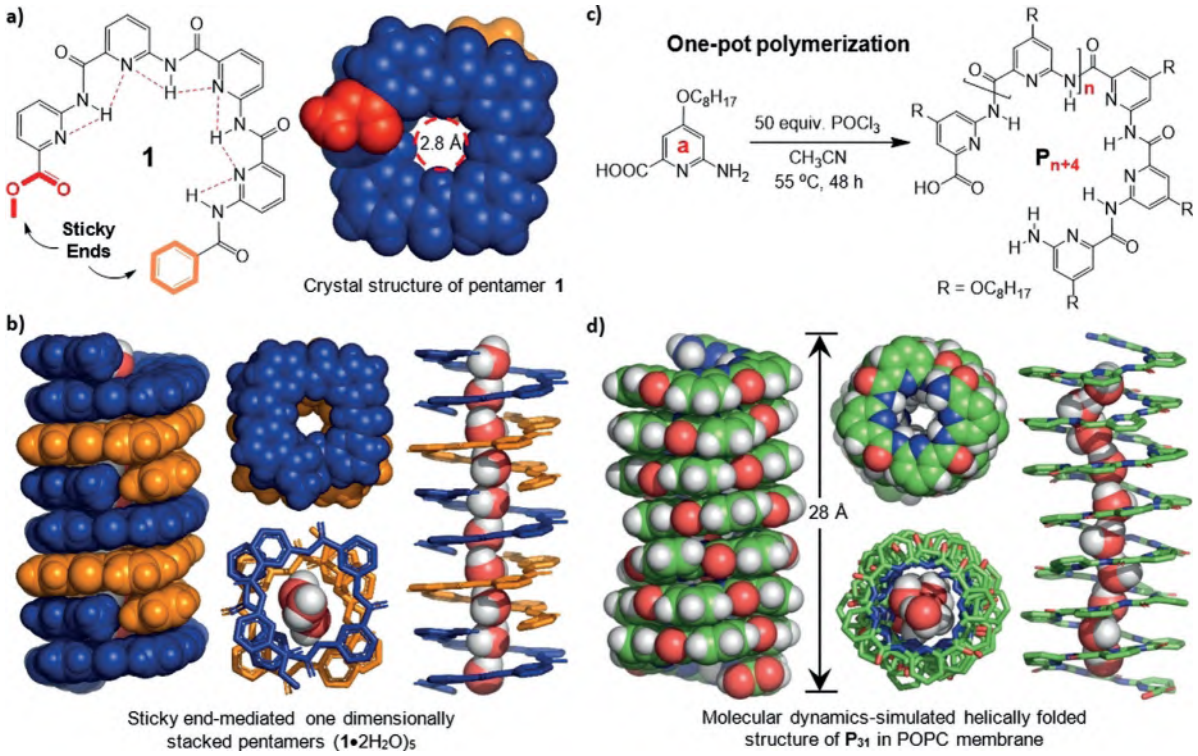

Figure 1. a) Structure of the helically folded pentamer **1** that contains two sticky ends (red and orange). b) Sticky-end-mediated noncovalent formation of the nanotubular structure $(\mathbf{1}\cdot 2H_2O)_5$ that contains a hollow nanopore of 2.8 Å in diameter for trapping hydrogen-bonded 1D water chain. c) One-pot synthesis of hydrogen-bonded amide-linked polypyridine polymers $\mathbf{P}_n$. d) Molecular dynamics simulated structure of $\mathbf{P}_{31}$ in POPC membrane, revealing the ability of polypyridine to host 1D water chains for possible transport of protons and water molecules.

ends, numerous molecules of **1** self-assemble, by intermolecular hydrogen bonds among the sticky ends, into a one-dimensionally stacked nanotubular structure, which is capable of accommodating a hydrogen-bonded single-file water chain in the hollow cavity (Figure 1b). This finding suggests a possible use of longer versions as selective synthetic water channels, allowing transport of water and protons, but not ions. Nevertheless, with an overall yield of less than 1% for pyridine pentamers that possess a helical height of 3.4 Å, generating longer versions for spanning the hydrophobic membrane region requires more than or equal to 30 repeating pyridine units and thus is synthetically difficult.

In this work, we have overcome this synthetic difficulty by the use of phosphoryl chloride ($POCl_3$) as a simple yet effective amide coupling agent, which mediates efficient one-pot polymerization reactions to generate helically folded polypyridine amide foldamers with an average helical height of 2.8 nm (Figure 1c,d). To the best of our knowledge, this is the first example of fully hydrogen-bonded aromatic amide foldamer-based long ONTs of greater than 1 nm, which are rapidly made from their constituent folding codons by a one-pot polymerization. Having a tubular cavity of about 2.8 Å and a length of 2.8 nm, these ion-rejecting polypyridine channels promote rapid and highly selective transport of 1.6×10^9 water molecules per second, a speed that exceeds the existing highly selective synthetic water channels by greater than 30-fold,[9f,10] and transport of protons as fast as gramicidin A (gA).

Results and Discussion

One-Pot Synthesis of Polymers P_{30} to P_{32}

Very recently, we showed that seven types of amide coupling agents (BOP, HATU, HBTU, TBTU, TOTU, DEPBT, and DMTMM) can be applied to prepare fully hydrogen-bonded aromatic hydrazide polymers, of a helical height of greater than 3 nm, from their repeating monomer units.[11] Under identical reaction conditions, however, we found these amide coupling agents, together with many others such as PyBroP, TATU, TCTU, TSTU, HCTU, and TFFH, do not yield even trace amounts of the fully hydrogen-bonded aromatic amide polymers $\mathbf{P}_n$, leaving starting materials (**a**) largely unreacted (Figure 1c). These comparative observations are consistent with the hydrogen-bonded hydrazide-linked aromatic backbone being less rigid than the similarly hydrogen-bonded amide-linked aromatic backbone.

Earlier on, we also showed that two equivalents of $POCl_3$ allow highly efficient one-pot synthesis of fully hydrogen-bonded near-planar macrocyclic amide pentamers at room temperature,[12a–c] and distorted hexamers or heptamers at high temperature.[12d] Encouraged by these findings, we tested polymerization efficacy of $POCl_3$ at different temperatures. We found that the use of either two or four equivalents of $POCl_3$ did not generate detectable amounts of the polymers $\mathbf{P}_n$ at up to 85 °C. But upon increasing $POCl_3$ to 25 equivalents, $\mathbf{P}_n$, having a number-average molecular weight (M_n) of

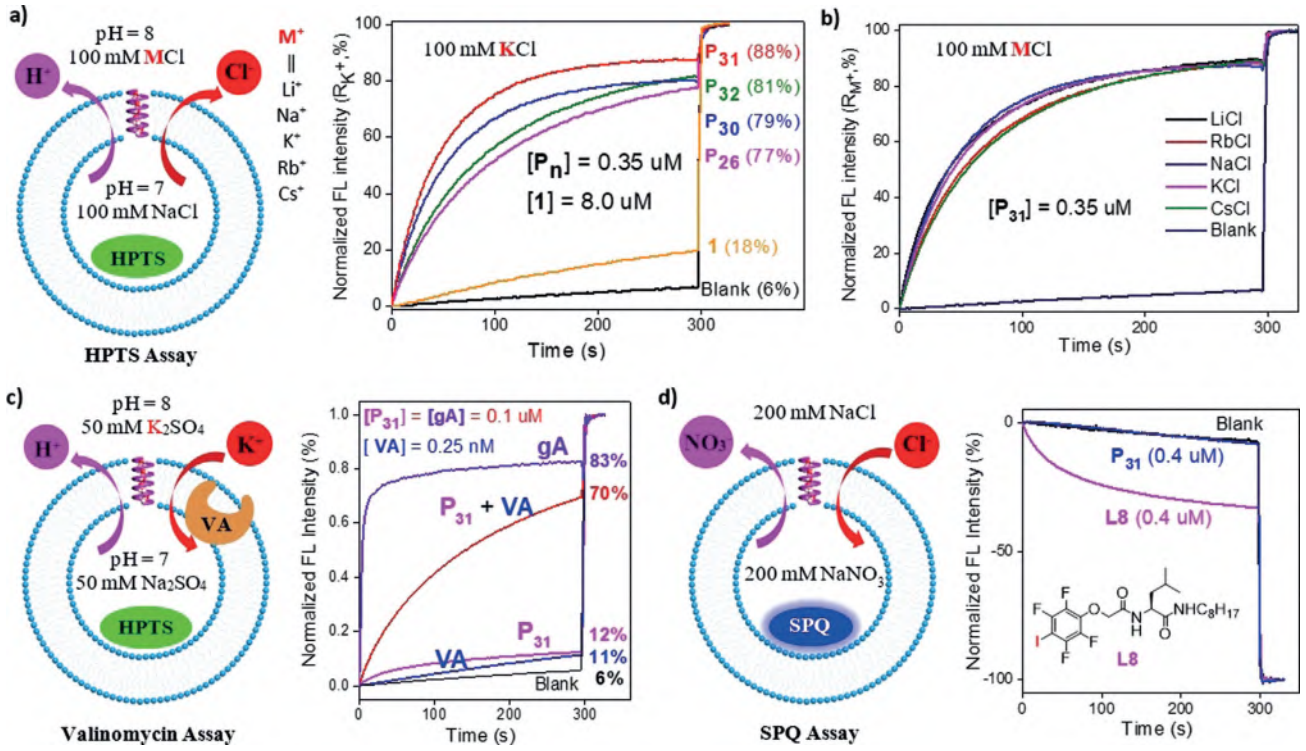

Figure 2. a,b) The pH-sensitive HPTS assay for assessing ion-transport activities of polypyridine-based channels $\mathbf{P}_n$ in EYPC-based LUVs. Fractional ion transport activities R_{M^+}, with the extravesicular region containing 100 mM MCl (M = Li, Na, K, Rb and Cs), were calculated using the equation $R_{M^+} = (I_{M^+} - I_0)/(I_{triton} - I_0)$, wherein I_{M^+} and I_0 (background intensity) are the ratiometric values of I_{460}/I_{403} at $t = 300$ s before addition of triton and I_{triton} is the ratiometric value of I_{460}/I_{403} at $t = 300$ s right after addition of triton. c) Valinomycin-based HPTS assay confirming K^+ to not be the positively charged species that is transported by $\mathbf{P}_{31}$. d) Chloride-sensitive SPQ assay, demonstrating that $\mathbf{P}_{31}$ does not transport anions. In (a) and (b), [total lipid] = 31 μM. Valinomycin = VA.

6.6 kDa, a polydispersity index value (PDI) of 1.97 (see Figures S1 and S2 and Table S1), 26.6 repeating **a** units (referred to as $\mathbf{P}_{27}$), and a tube length of 2.4 nm, were produced at yield of around 40% at 55 °C (entry 3, Table S1). Further increasing $POCl_3$ to 50 equivalents or the temperature to 85 °C increases M_n to 7.6, 7.7, and 7.9 kDa, referred to as $\mathbf{P}_{30}$, $\mathbf{P}_{31}$, and $\mathbf{P}_{32}$, respectively, with corresponding lengths of 2.8, 2.8, and 3.0 nm and PDI values of less than 2 (see Figures S3–S8 and Table S1).

Ion-Transport Properties of Polymers P_{30} to P_{32}

Employing EYPC-based large unilamellar vesicles (LUVs) and the pH-sensitive HPTS assay (Figure 2a), the fractional ion-transport activities of the polymers $\mathbf{P}_n$ were measured and found to increase on the order of $\mathbf{P}_{27} < \mathbf{P}_{30} < \mathbf{P}_{32} < \mathbf{P}_{31}$. That is, $\mathbf{P}_{31}$ of 2.8 nm in helical height, which was obtained at yield of 50% using 50 equivalents of $POCl_3$ at 55 °C, performed the best among the four polymer samples, all of which are far more active than the pentamer **1**. Based on the Hill analysis, the EC_{50} value of $\mathbf{P}_{31}$ was determined to be 0.2 μM or 0.65 mol% relative to lipids (see Figure S9).

P_{31}-Mediated Transport Proceeds with High Selectivity

In principle, four possible ion-exchange processes, that is, M^+/H^+ antiport, X^-/OH^- antiport, M^+/OH^- symport, or X^-/H^+ symport, could account for the ion-transport activities seen in the HPTS assay (Figure 2a). Since $\mathbf{P}_{31}$, having an average nanotube length of 2.8 nm, exhibits the highest transport activity among the four polymer samples studied, we subsequently employed it in a range of lipid bilayer experiments to investigate the most likely transport species/mechanism for $\mathbf{P}_n$-mediated ion transport.

First, we used the same HPTS assay shown in Figure 2a, but systematically varied the extravesicular salts MCl (M = Li, Na, K, Rb, and Cs). Results summarized in Figure 2b demonstrate that $\mathbf{P}_{31}$-mediated ion-transport activities are MCl-independent, pointing to the inability of $\mathbf{P}_{31}$ to transport cations M^+.

Next, we conducted a valinomycin (VA, a K^+ carrier) based HPTS assay where 50 mM M_2SO_4 was used to replace 100 mM MCl to eliminate any possible influences from chloride anions through passive membrane diffusion (Figure 2c). If K^+ transport, which is mediated either by $\mathbf{P}_{31}$ or simply through passive membrane diffusion, is a rate-limiting step, addition of VA will speed up the transmembrane movement of K^+ ions and subsequently proton transport, consequently resulting in enhanced fluorescence intensity of HPTS. Experimentally, after normalization using $R_{K^+} =$

$(I_{K^+}-I_0)/(100\%-I_0)$, we obtained R_{K^+} values of 68% in the presence of VA and 6.4% in the absence of VA. Since the fluorescence intensity for VA alone is only 5.3%, a large difference by 61.6% unambiguously confirms either protons or hydroxides, and definitely not K^+ ions, to be the molecular species transported by $\mathbf{P_{31}}$. Encouraged by the findings from this VA assay, we studied the transport behavior $\mathbf{P_{31}}$ using the HPTS assay at pH 7, having no salt in the intravesicular region, but with either Na_2SO_4 or K_2SO_4 as high as 200 mM in the extravesicular region (see Figure S10). Under these conditions, while gA, which can transport H^+, Na^+, and K^+ ions, elicits 100% transport activity within 6 seconds at 0.1 μM, $\mathbf{P_{31}}$ displays no detectable activities even after 300 seconds at 0.4 μM. These results lend additional support to the notion that $\mathbf{P_{31}}$ lacks the ability to transport metal ions, including Na^+ and K^+.

To probe the role played by anions, X^-, we carried out a chloride-sensitive SPQ assay (Figure 2d). SPQ is a fluorescent chloride indicator, with fluorescence decreasing upon increasing Cl^- concentration. Hence, if $\mathbf{P_{31}}$ can mediate chloride influx into LUVs, decrease in fluorescence intensity of SPQ is expected. With this assay, although we did not observe any change in fluorescence intensity in the presence of $\mathbf{P_{31}}$ at 0.4 μM, we did obtain 33% quenching of the SPQ dye in the presence of the anion channel **L8**[16] at 0.4 μM. These data confirm that $\mathbf{P_{31}}$ does not transport anions.

In addition, a high transport activity observed with the NaCl/KCl system (R_{K^+} = 87%, Figure 2b) vs. a low transport activity of 15% with the Na_2SO_4/K_2SO_4 system (see Figure S11a) suggests the $\mathbf{P_{31}}$-mediated proton efflux to be predominantly accompanied by the passive efflux of Cl^-, and to some extent the metal ions, to maintain a charge neutrality of the system. This likelihood can be corroborated by the fact that metal ions such as Na^+ apparently are much less permeable than Cl^- (see Figure S11b vs. S11c).

P_{31} Transports Protons with High Selectivity through a Channel Mechanism

At present, we cannot differentiate $\mathbf{P_n}$-mediated transport of H^+ from that of OH^-. Nevertheless, given a well-defined hydrogen-bonded water chain present in $\mathbf{P_n}$, rapid transport of H^+ through a Grotthuss mechanism certainly is a possibility far more likely than transport of OH^- through the water chain. Given that the interior cavity of $\mathbf{P_n}$ is as small as 2.8 Å in diameter and contains no binding groups for sufficiently compensating the dehydration energy of ions (Na^+, K^+, Cl^-, etc), we also anticipate high preference in proton transport over transport of other ions (Na^+, K^+, Cl^-, etc). To provide conclusive evidence, we recorded single-channel current traces for $\mathbf{P_{31}}$ using symmetrical and unsymmetrical baths (Figures 3; see Figures S12 and S13).

As illustrated in Figure 3a, in symmetrical baths (i.e., *cis* chamber = *trans* chamber = 0.25 M HCl), we observed well-defined single-channel current traces that are supportive of proton-conducting channel activities of $\mathbf{P_{31}}$ at the single-channel level. Further, by plotting current traces versus

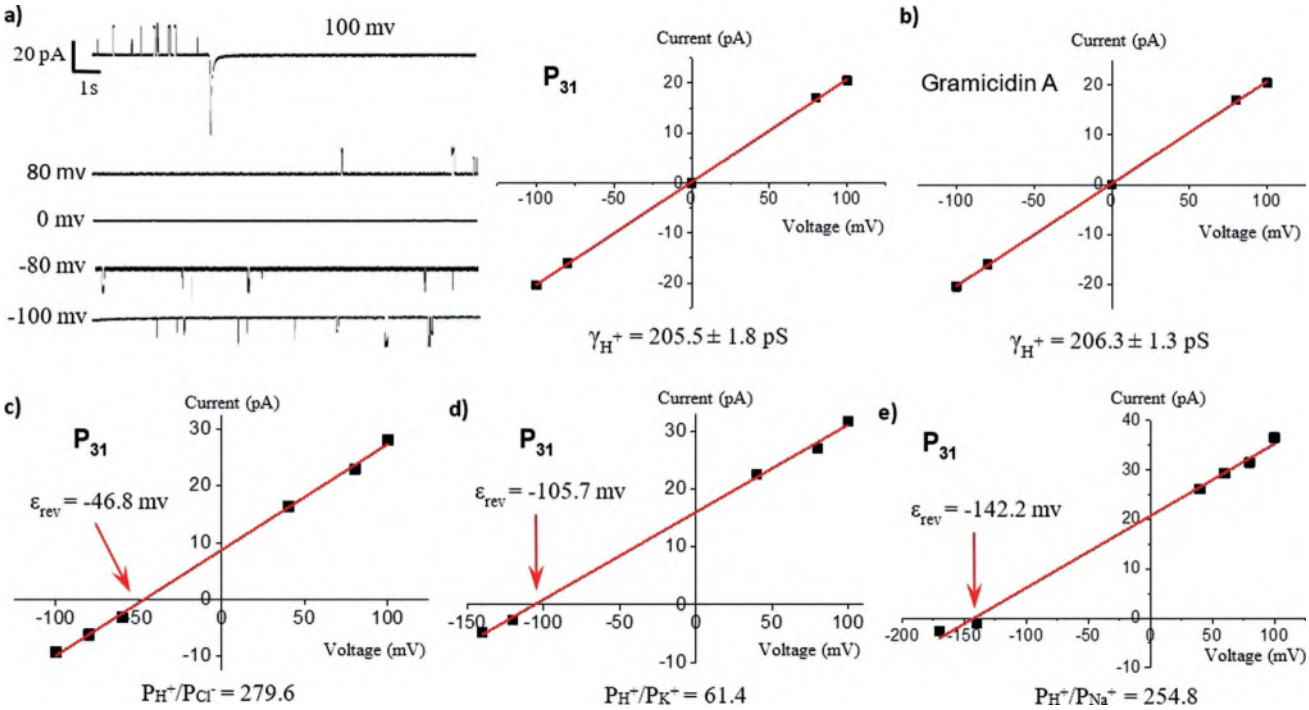

Figure 3. a) Single current traces of $\mathbf{P_{31}}$ recorded in the planar lipid bilayer in symmetrical 0.25 M HCl solutions (*cis* chamber = *trans* chamber = 0.25 M HCl) for determining proton conduction rate (γ_{H^+}) for $\mathbf{P_{31}}$. b) The determined γ_{H^+} value for gramicidin. c–e) *I–V* curves and determined ion selectivity ratios of P_{H^+}/P_{Cl^-}, P_{H^+}/P_{K^+}, and P_{H^+}/P_{Na^+} for $\mathbf{P_{31}}$. In (c), permeability ratio of P_{H^+}/P_{Cl^-} was obtained by fitting the *I–V* curve using the simplified Goldman-Hodgkin-Katz equation ($\varepsilon_{rev} + 23.5 = RT/F\ln\{(P_{H^+}[H^+]_{trans} + P_{Cl^-}[Cl^-]_{cis})/(P_{H^+}[H^+]_{cis} + P_{Cl^-}[Cl^-]_{trans})\}$). For (d) and (e), the corresponding equation is $\varepsilon_{rev} = RT/F\ln(P_{M^+}/P_{H^+})$. Here, 23.5 mV is the Nernst potential that corresponds to a proton gradient of 0.10 M to 0.25 M, R = universal gas constant (8.314 $JK^{-1}mol^{-1}$), T = 300 K, F = Faraday's constant (96485 $Cmol^{-1}$).

voltages, we obtained a proton conduction rate (γ_{H^+}) of 205.5 ± 1.8 pS, a proton conduction rate that is near-identical to the γ_{H^+} value for gA (206.3 ± 1.3 pS, Figure 3b; see Figure S12a), indicating the water chains inside $\mathbf{P_{31}}$ is optimized as that in gA for rapid conduction of protons across membrane by a Grotthuss mechanism.

To determine H^+/Cl^- transport selectivity (i.e., P_{H^+}/P_{Cl^-}) at the single-channel level, we further recorded single-channel current traces for $\mathbf{P_{31}}$ in unsymmetrical baths (*cis* chamber = 0.25 M HCl and *trans* chamber = 0.10 M HCl; see Figure S12b). Curve fitting yields a reverse potential value of −46.8 mV (ε_{rev}, Figure 3c). After further considering the Nernst potential of proton gradient from 0.10 to 0.25 M, substituting this reverse potential value into a simplified Goldman-Hodgkin-Katz equation (see Figure 3c) gives a H^+/Cl^- ion selectivity value of 279.6.

Similarly, based on the respective ε_{rev} values of −105.7 mV and −142.2 mV (Figure 3d,e; see Figure S13), H^+/K^+ and H^+/Na^+ ion selectivity values were determined to be 61.4 and 254.8, respectively.

Among the three ions (Na^+, K^+, and Cl^-), Cl^- is the least permeable, likely due to its largest ionic diameter of 3.5 Å that is much larger than the pore diameter of 2.8 Å of $\mathbf{P_{31}}$. In contrast, K^+, having a dehydration energy (83.0 kcal mol^{-1}) smaller than that of Na^+ (105.0 kcal mol^{-1}) and an ionic diameter of 2.8 Å, which still fits into the cavity of $\mathbf{P_{31}}$, becomes the most permeable among the three ions.

P_{31} Mediates Rapid Water Transport with High Selectivity

The presence of a hydrogen-bonded one-dimensional (1D) water chain in $\mathbf{P_{31}}$ suggests its ability to conduct water transport. Using a stopped flow instrument, we studied its water-transport properties in the widely used DOPC (1,2-dioleoyl-sn-glycero-3-phosphocholine lipid) membrane, which has a hydrophobic thickness of 2.7 nm,[17] thus matches the nanotubular length of 2.8 nm of $\mathbf{P_{31}}$.

We premixed DOPC lipids and $\mathbf{P_{31}}$ at different lipid/channel molar ratios of 2000:1 to 8000:1 in chloroform, from which about 120 nm LUVs were prepared in a 10 mM HEPES buffer (100 mM NaCl, pH 7.0) and exposed to a hypertonic osmolyte (300 mM sucrose) in the same HEPES buffer. Water efflux results in vesicle shrinkage and subsequent increase in light scattering intensity (see Figure S14). Based on time-dependent changes in light scattering, we derived the water permeability (*Pf* in units of cm s^{-1}) of vesicles in the absence and presence of $\mathbf{P_{31}}$. To obtain single-channel insertion efficiency, we first measured the actual lipid concentrations before and after extrusion, and found that 25% lipid was lost after extrusion (see Figure S15). This measurement was followed by comparing the fluorescence intensity of $\mathbf{P_{31}}$ at 439 nm (see Figure S16) to yield the actual lipid/channel molar ratio after extrusion and an accurate number of single-channels present in the LUVs (Table S2). With these single-channel insertion efficiencies, and after subtracting the background permeability, we obtained the single-channel permeability, *Pw* (in the unit of cm^3 s^{-1}), for $\mathbf{P_{31}}$ at various lipid/channel molar ratios (Figure 4a; see Table S3).

Channel $\mathbf{P_{31}}$ exhibits water permeability as high as 4.81 ± 0.17 × 10^{-14} cm^3 s^{-1} at a lipid/channel molar ratio of 6000:1. This value, corresponding to a rapid water transport of 1.6 × 10^9 H_2O·s^{-1}·channel^{-1}, is more than 30 times as fast as currently available highly selective synthetic water channel.[9f,10]

In contrast, channel **1**, which is also capable of forming 1D water-chain-containing nanotubes by self-assembly (Figure 1b), displays a marginal water permeability of 0.66 ± 0.12 × 10^{-14} cm^3 s^{-1} (2.2 × 10^8 water molecules s^{-1}; see Table S3 and Figure S17b). In further comparison, water-chain-containing gA gives a relatively low water permeability of 1.95 ± 0.11 × 10^{-14} cm^3 s^{-1} (6.5 × 10^8 H_2O·s^{-1}·channel^{-1}; see Table S3 and Figure S17b), a value that is in good accord with the permeability value of 1.6 ± 0.3 × 10^{-14} cm^3 s^{-1} recently reported.[14]

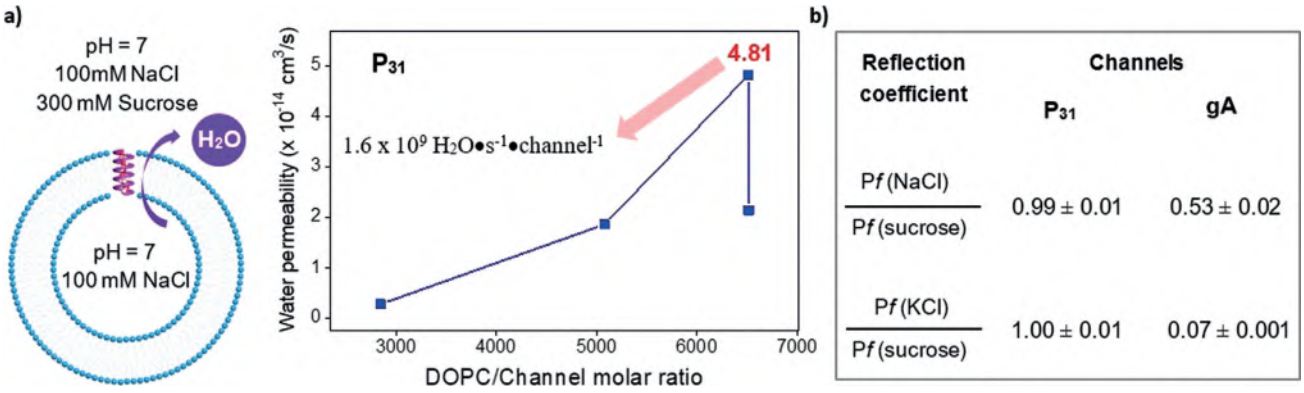

Figure 4. a) DOPC-based LUVs under hypertonic conditions (300 mM sucrose) for quantifying water permeability of the channels $\mathbf{P_{31}}$ at different lipid/channel molar ratios. b) Comparative water permeability ratios measured using three types of hypertonic conditions (300 mM sucrose, 250 mM NaCl or 250 mM KCl), unambiguously establishing near-complete and incomplete salt rejections by $\mathbf{P_{31}}$ and gA, respectively. All the values were obtained over three independent runs.

Using Arrhenius plots that correlate water permeability with temperature, the activation energies (E_a) were determined to be 8.89 ± 0.20 and 12.19 ± 0.20 kcal mol^{-1} for LUVs in the presence and absence, respectively, of $\mathbf{P_{31}}$ (see Figure S17c).

The above lipid bilayer experiments (Figures 2b–d; see Figure S3) and single-channel current measurements (Figure 3c–e) suggest $\mathbf{P_{31}}$-mediated water transport should occur with high salt rejections. To examine the water-transport selectivity, water permeability (P_f) values of the vesicles were measured under three hypertonic conditions, that is, 300 mM sucrose, 150 mM NaCl, and 150 mM KCl.[15] For water channels that exhibit high rejection of NaCl and KCl, P_f values measured in either NaCl or KCl should be close to that in sucrose. In other words, if we define reflection coefficients as a ratio of P_f values [e.g., P_f (NaCl)/P_f (sucrose) or P_f (KCl)/P_f (sucrose)], both reflection coefficients should be close to 1 for highly selective water transport.

Indeed, for the polypridine channel $\mathbf{P_{31}}$, we obtained reflection coefficients of 0.99 ± 0.01 for P_f (NaCl)/P_f (sucrose) and of 1.00 ± 0.01 for P_f (KCl)/P_f (sucrose) (Figure 4b), thereby confirming that $\mathbf{P_{31}}$ transports water molecules not only at a high speed but also with high salt rejection. The reliability of the method can be corroborated by low reflection coefficients of 0.53 ± 0.02 for P_f (NaCl)/P_f (sucrose) and 0.07 ± 0.001 for P_f (KCl)/P_f (sucrose) in the case of the channel gA (Figure 4b), which is known to rapidly transport both Na^+ and K^+ as further demonstrated in Figure S10.

Conclusion

To summarize, we have established the use of $POCl_3$ as a simple and effective one-pot polymerization agent for efficient preparation of fully hydrogen-bonded aromatic amide foldamer-based helically folded organic nanotubes of 2.8 nm in length. This report is the first of such a unique class of organic nanotubes, having a sufficiently long backbone for spanning the hydrophobic membrane region, being efficiently made by a one-pot polymerization from their constituent hydrogen-bonded helicity codons. Apart from this unprecedented one-pot polymerization protocol, we have further demonstrated good use of such foldamer-based nanotubes in mediating rapid transport of both protons and water with near-perfect selectivity. Notably, the proton-transport speed matches the very high level exhibited by gramicidin A, and the water permeability exceeds the currently available highly selective synthetic water channels by at least 30-fold.[9f,10] Given the availability of wide-ranging helicity codons for creating helically folded aromatic amide foldamers that possess a hollow cavity of up to 30 Å across,[5f–i] our $POCl_3$-based one-pot polymerization protocol, together with other acylating agents to be explored, may enable rapid access to exceptionally diverse types of fully hydrogen-bonded aromatic amide foldamer-based organic nanotubes with hollow tubular cavities that are widely and precisely adjustable for multidisciplinary applications at the interface of chemistry, materials science, medicine, and biology.

Acknowledgements

This work is supported by the NanoBio Lab (Biomedical Research Council, Agency for Science, Technology and Research, Singapore).

Conflict of interest

The authors declare no conflict of interest.

Keywords: Foldamers · helical structures · hydrogen bonds · nanotubes · supramolecular chemistry

[1] a) M. A. B. Block, C. Kaiser, A. Khan, S. Hecht, *Top. Curr. Chem.* **2005**, *245*, 89–150; b) B. Gong, Z. Shao, *Acc. Chem. Res.* **2013**, *46*, 2856–2866; c) S. Doninelli, M. Badoux, A. F. M. Kilbinger in *Bio-inspired Polymers* (Eds.: N. Bruns, A. F. M. Kilbinger), The Royal Society of Chemistry, The United Kingdom, **2016**, pp. 141–220; d) D.-W. Zhang, H. Wang, Z.-T. Li, *Macromol. Rapid Commun.* **2017**, *38*, 1700179; e) C.-Z. Liu, M. Yan, H. Wang, D.-W. Zhang, Z.-T. Li, *ACS Omega* **2018**, *3*, 5165–5176; f) Y. Ferrand, I. Huc, *Acc. Chem. Res.* **2018**, *51*, 970–977; g) D. T. Bong, T. D. Clark, J. R. Granja, M. R. Ghadiri, *Angew. Chem. Int. Ed.* **2001**, *40*, 988–1011; *Angew. Chem.* **2001**, *113*, 1016–1041; h) S. Matile, *Chem. Soc. Rev.* **2001**, *30*, 158–167; i) J. G. Rudick, V. Percec, *Acc. Chem. Res.* **2008**, *41*, 1641–1652; j) I. W. Hamley, *Angew. Chem. Int. Ed.* **2014**, *53*, 6866–6881; *Angew. Chem.* **2014**, *126*, 6984–7000; k) T. G. Barclay, K. Constantopoulos, J. Matisons, *Chem. Rev.* **2014**, *114*, 10217–10291; l) Y. P. Huo, H. Q. Zeng, *Acc. Chem. Res.* **2016**, *49*, 922–930; m) T. Shimizu, *Bull. Chem. Soc. Jpn.* **2018**, *91*, 623–668.

[2] a) T. D. Clark, M. R. Ghadiri, *J. Am. Chem. Soc.* **1995**, *117*, 12364–12365; b) Y. Xu, M. D. Smith, M. F. Geer, P. J. Pellechia, J. C. Brown, A. C. Wibowo, L. S. Shimizu, *J. Am. Chem. Soc.* **2010**, *132*, 5334–5335; c) S. Rondeau-Gagné, J. R. Néabo, M. Desroches, J. Larouche, J. Brisson, J.-F. Morin, *J. Am. Chem. Soc.* **2013**, *135*, 110–113; d) S. Hecht, A. Khan, *Angew. Chem. Int. Ed.* **2003**, *42*, 6021–6024; *Angew. Chem.* **2003**, *115*, 6203–6206; e) K. Maeda, L. Hong, T. Nishihara, Y. Nakanishi, Y. Miyauchi, R. Kitaura, N. Ousaka, E. Yashima, H. Ito, K. Itami, *J. Am. Chem. Soc.* **2016**, *138*, 11001–11008; f) Y. Kim, M. F. Mayer, S. C. Zimmerman, *Angew. Chem. Int. Ed.* **2003**, *42*, 1121–1126; *Angew. Chem.* **2003**, *115*, 1153–1158.

[3] a) J.-L. Schmitt, J.-M. Lehn, *Helv. Chim. Acta* **2003**, *86*, 3417–3426; b) J. Zhu, Z. Dong, S. Lei, L. Cao, B. Yang, W. Li, Y. Zhang, J. Liu, J. Shen, *Angew. Chem. Int. Ed.* **2015**, *54*, 3097–3101; *Angew. Chem.* **2015**, *127*, 3140–3144; c) F. Chen, J. Shen, N. Li, A. Roy, R. J. Ye, C. L. Ren, H. Q. Zeng, *Angew. Chem. Int. Ed.* **2020**, *59*, 1440–1444; *Angew. Chem.* **2020**, *132*, 1456–1460.

[4] a) Y. Hamuro, S. J. Geib, A. D. Hamilton, *Angew. Chem. Int. Ed. Engl.* **1994**, *33*, 446; *Angew. Chem.* **1994**, *106*, 465; b) J. Zhu, R. D. Parra, H. Q. Zeng, E. Skrzypczak-Jankun, X. C. Zeng, B. Gong, *J. Am. Chem. Soc.* **2000**, *122*, 4219–4220; c) V. Berl, I. Huc, R. G. Khoury, M. J. Krische, J. M. Lehn, *Nature* **2000**, *407*, 720–723.

[5] a) B. Gong, *Chem. Eur. J.* **2001**, *7*, 4336–4342; b) I. Huc, *Eur. J. Org. Chem.* **2004**, 17–29; c) I. Saraogi, A. D. Hamilton, *Chem. Soc. Rev.* **2009**, *38*, 1726–1743; d) G. Guichard, I. Huc, *Chem. Commun.* **2011**, *47*, 5933–5941; e) K. Yamato, M. Kline, B. Gong, *Chem. Commun.* **2012**, *48*, 12142–12158; f) D.-W. Zhang, X. Zhao, J.-L. Hou, Z.-T. Li, *Chem. Rev.* **2012**, *112*, 5271–5316; g) W. Q. Ong, H. Q. Zeng, *J. Inclusion Phenom. Macrocyclic*

Chem. **2013**, *76*, 1 – 11; h) H. L. Fu, Y. Liu, H. Q. Zeng, *Chem. Commun.* **2013**, *49*, 4127; i) B. Gong, H. Q. Zeng, J. Zhu, L. H. Yuan, Y. H. Han, S. Z. Cheng, M. Furukawa, R. D. Parra, A. Y. Kovalevsky, J. L. Mills, E. Skrzypczak-Jankun, S. Martinovic, R. D. Smith, C. Zheng, T. Szyperski, X. C. Zeng, *Proc. Natl. Acad. Sci. USA* **2002**, *99*, 11583 – 11588.

[6] a) S. H. Gellman, *Acc. Chem. Res.* **1998**, *31*, 173 – 180; b) D. J. Hill, M. J. Mio, R. B. Prince, T. S. Hughes, J. S. Moore, *Chem. Rev.* **2001**, *101*, 3893 – 4011.

[7] S. J. Dawson, Á. Mészáros, L. Pethő, C. Colombo, M. Csékei, A. Kotschy, I. Huc, *Eur. J. Org. Chem.* **2014**, 4265 – 4275.

[8] J. Cao, M. Kline, Z. Chen, B. Luan, M. Lv, W. Zhang, C. Lian, Q. Wang, Q. Huang, X. Wei, J. Deng, J. Zhu, B. Gong, *Chem. Commun.* **2012**, *48*, 11112 – 11114.

[9] a) W. Q. Ong, H. Q. Zhao, Z. Y. Du, J. Z. Y. Yeh, C. L. Ren, L. Z. W. Tan, K. Zhang, H. Q. Zeng, *Chem. Commun.* **2011**, *47*, 6416 – 6418; b) W. Q. Ong, H. Q. Zhao, C. Sun, J. E. Wu, Z. C. Wong, S. F. Y. Li, Y. H. Hong, H. Q. Zeng, *Chem. Commun.* **2012**, *48*, 6343 – 6345; c) H. Q. Zhao, W. Q. Ong, F. Zhou, X. Fang, X. Y. Chen, S. F. Y. Li, H. B. Su, N.-J. Cho, H. Q. Zeng, *Chem. Sci.* **2012**, *3*, 2042 – 2046; d) W. Q. Ong, H. Q. Zhao, X. Fang, S. Woen, F. Zhou, W. L. Yap, H. B. Su, S. F. Y. Li, H. Q. Zeng, *Org. Lett.* **2011**, *13*, 3194 – 3197; e) H. Q. Zhao, W. Q. Ong, X. Fang, F. Zhou, M. N. Hii, S. F. Y. Li, H. B. Su, H. Q. Zeng, *Org. Biomol. Chem.* **2012**, *10*, 1172 – 1180; f) H. Q. Zhao, S. Sheng, Y. H. Hong, H. Q. Zeng, *J. Am. Chem. Soc.* **2014**, *136*, 14270 – 14276.

[10] a) M. S. Kaucher, M. Peterca, A. E. Dulcey, A. J. Kim, S. A. Vinogradov, D. A. Hammer, P. A. Heiney, V. Percec, *J. Am. Chem. Soc.* **2007**, *129*, 11698 – 11699; b) Y. L. Duc, M. Michau, A. Gilles, V. Gence, Y.-M. Legrand, A. Lee, S. Tingry, M. Barboiu, *Angew. Chem. Int. Ed.* **2011**, *50*, 11366; *Angew. Chem.* **2011**, *123*, 11568; c) X. B. Zhou, G. D. Liu, K. Yamato, Y. Shen, R. X. Cheng, X. X. Wei, W. L. Bai, Y. Gao, H. Li, Y. Liu, F. T. Liu, D. M. Czajkowsky, J. F. Wang, M. J. Dabney, Z. H. Cai, J. Hu, F. V. Bright, L. He, X. C. Zeng, Z. F. Shao, B. Gong, *Nat. Commun.* **2012**, *3*, 949; d) C. B. Hu, Z. X. Chen, G. F. Tang, J. L. Hou, Z. T. Li, *J. Am. Chem. Soc.* **2012**, *134*, 8384 – 8387; e) E. Licsandru, I. Kocsis, Y.-x. Shen, S. Murail, Y.-M. Legrand, A. van der Lee, D. Tsai, M. Baaden, M. Kumar, M. Barboiu, *J. Am. Chem. Soc.* **2016**, *138*, 5403 – 5409; f) Y.-x. Shen, W. Si, M. Erbakan, K. Decker, R. De Zorzi, P. O. Saboe, Y. J. Kang, S. Majd, P. J. Butler, T. Walz, A. Aksimentiev, J.-l. Hou, M. Kumar, *Proc. Natl. Acad. Sci. USA* **2015**, *112*, 9810 – 9815; g) I. Kocsis, M. Sorci, H. Vanselous, S. Murail, S. E. Sanders, E. Licsandru, Y.-M. Legrand, A. van der Lee, M. Baaden, P. B. Petersen, G. Belfort, M. Barboiu, *Sci. Adv.* **2018**, *4*, eaao5603; h) R. H. Tunuguntla, R. Y. Henley, Y.-C. Yao, T. A. Pham, M. Wanunu, A. Noy, *Science* **2017**, *357*, 792 – 796.

[11] A. Roy, H. Joshi, R. J. Ye, J. Shen, F. Chen, A. Aksimentiev, H. Q. Zeng, *Angew. Chem. Int. Ed.* **2020**, *59*, 4806 – 4813; *Angew. Chem.* **2020**, *132*, 4836 – 4843.

[12] a) B. Qin, W. Q. Ong, R. J. Ye, Z. Y. Du, X. Y. Chen, Y. Yan, K. Zhang, H. B. Su, H. Q. Zeng, *Chem. Commun.* **2011**, *47*, 5419 – 5421; b) B. Qin, C. Sun, Y. Liu, J. Shen, R. J. Ye, J. Zhu, X.-F. Duan, H. Q. Zeng, *Org. Lett.* **2011**, *13*, 2270 – 2273; c) B. Qin, S. Shen, C. Sun, Z. Y. Du, K. Zhang, H. Q. Zeng, *Chem. Asian J.* **2011**, *6*, 3298 – 3305; d) Y. Liu, B. Qin, H. Q. Zeng, *Sci. China Chem.* **2012**, *55*, 55 – 63.

[13] The water transport rate of channel $\mathbf{P_{31}}$ was caculated to be 0.7×10^9 $H_2O{\cdot}s^{-1}{\cdot}channel^{-1}$ by using Pohl's new equation. For this new equation, see: C. Hannesschläger, T. Barta, C. Siligan, A. Horner, *Sci. Rep.* **2018**, *8*, 8516.

[14] P. Pohl, S. M. Saparov, *Biophys. J.* **2000**, *78*, 2426 – 2434.

[15] A. K. Meinild, D. A. Klaerke, T. Zeuthen, *J. Biol. Chem.* **1998**, *273*, 32446 – 32451.

[16] C. Ren, X. Ding, A. Roy, J. Shen, S. Zhou, F. Chen, S. F. Yau Li, H. Ren, Y. Y. Yang, H. Zeng, *Chem. Sci.* **2018**, *9*, 4044 – 4051.

[17] Y. Guo, S. Pogodin, V. A. Baulin, *J. Chem. Phys.* **2014**, *140*, 174903.

Manuscript received: March 7, 2020
Revised manuscript received: April 10, 2020
Accepted manuscript online: April 28, 2020
Version of record online: May 28, 2020

